A Theory for Electric Dichroism and Birefringence Decays and Depolarized Dynamic Light Scattering of Weakly Bending Rods

Patrick J. Heath,† Stuart A. Allison,‡ John A. Gebe,† and J. Michael Schurr*,†

Department of Chemistry, BG-10, University of Washington, Seattle, Washington 98195, and Department of Chemistry, Georgia State University, Atlanta, Georgia 30303

Received December 28, 1994; Revised Manuscript Received June 13, 1995®

ABSTRACT: When a weakly bending rod consisting of discrete subunits is partially oriented in a weak electric field by an independent induced dipole mechanism, the off-field decay of its dichroism or birefringence reflects the same mutual-rotational correlation function that is manifested in its forward depolarized dynamic light scattering. An analytical theory of that mutual-rotational correlation function is developed by extending a previous theory for self-rotational correlation functions of subunits in macromolecules with mean local cylindrical symmetry, and the result is formulated in terms of a previous normal mode theory for discrete weakly bending rods. Results from this analytical theory are compared with those of Brownian dynamics simulations with generally good agreement. By dissecting the analytical theory, explanations are found both for the unexpectedly small fraction of total relaxing amplitude that appears in the rapid initial transient due to bending and for the absence of the relaxation time of the longest bending mode from that initial relaxation.

Introduction

The flexural dynamics of weakly bending rodlike macromolecules are in principle accessible by a variety of optical methods that are sensitive to rotations of their constituent subunits. Subunit *self*-rotational correlation functions are measured by time-resolved emission or absorption polarization anisotropy under conditions where the signal on any given shot arises from at most one chromophore per rod.[1] Subunit *mutual*-rotational correlation functions are manifested in the off-field decays of transient electric dichroism and birefringence experiments, and in the zero-angle depolarized dynamic light scattering, as detailed below. The particular kind of mutual-rotational correlation function monitored in the electro-optic experiments actually depends on the orientation mechanism and strength of the applied electric field.[2,3] In any case, for a weakly bending rod, both the self- and mutual-rotational correlation functions exhibit a rapid initial decay associated with bending motions in addition to a larger amplitude of the main decay associated with the end-over-end tumbling motion of the rods, more precisely of an equilibrium ensemble of bent rods. It is the fast initial transient in these correlation functions that provides information regarding the dynamics of bending, whereas the main relaxation provides information about the extent of bending at equilibrium, or equivalently about the equilibrium persistence length, provided the contour length is known.

The bending dynamics in principle provide information that is not available from the equilibrium persistence length. For example, the bending rigidity itself might be a relaxing property, in which case the dynamic bending rigidity that governs flexural motions on a sufficiently short time scale would exceed that manifested in the equilibrium bending. Indeed, there are some indications that the dynamic bending rigidity of DNA on a time scale less than 10 μs may be 2−4-fold greater than the value inferred from the equilibrium persistence length,[4−6] although that issue is not yet completely resolved. It is also possible that internal friction, in addition to solvent friction, may retard the bending motions, in which case the *apparent* dynamic bending rigidity derived from experimental data would lie below the actual value, and possibly even below that inferred from the equilibrium persistence length. Investigations of the flexural dynamics of various rodlike and filamentous species are expected to become more numerous in the future, as bending problems attract increased attention.

Brownian dynamics simulations of discrete wormlike chains have proven quite useful in the interpretation of various experimental data.[2−4,7−9] Nevertheless, analytical theories (within their domains of validity) offer some advantages by providing model functions for iterative data fitting, and by providing a conceptual framework to deepen the level of analysis and understanding of the results. A normal mode theory for the Brownian dynamics of weakly bending rods was previously formulated[1] and incorporated into existing theory[10] for the *self*-rotational correlation functions that are probed by time-resolved optical anisotropy experiments. Detailed comparisons with corresponding Brownian dynamics simulations[1] established the domain of validity of that normal mode theory as $L/P_d \leq 0.6$, where L is the contour length and P is the persistence length corresponding to the dynamic bending rigidity, henceforth referred to as the dynamic persistence length.

The primary objective of the present work is to develop a corresponding analytical theory for subunit *mutual*-rotational correlation functions that applies to filaments with mean local cylindrical symmetry. Into that theory we shall incorporate certain results from the previous normal mode theory for weakly bending rods in order to evaluate the new correlation functions. Numerical results from this new analytical theory are then compared in detail with the corresponding results from Brownian dynamics simulations.

An approximate analytical theory has also been developed for treating the bending dynamics of considerably longer wormlike chains with L/P_d ratios up to 2.0 or more.[19−22] By incorporating certain results from recent versions of that theory[21,22] into the present

† University of Washington.
‡ Georgia State University.
® Abstract published in *Advance ACS Abstracts,* August 15, 1995.

0024-9297/95/2228-6600$09.00/0

formulation for the mutual correlation function, it should be possible to achieve useful analytical results that span the range of flexibility from rigid rods up to wormlike coils with as many as two to four persistence lengths. However, such a project lies beyond the scope of the present work.

There are two puzzling aspects to both previous[3] and present results for the relevant mutual correlation functions. First, the fraction of the total relaxation due to the bending motions (i.e. the fraction of rapid initial transient) is much smaller in the case of mutual correlation functions than in the case of the corresponding self-correlation functions. Secondly, the relative contribution of the longest ($l = 3$) bending normal mode, specifically of the term with the $1/\tau_3$ relaxation rate, to the rapid initial transient is greatly reduced in the case of the mutual correlation functions, so that it no longer dominates the fast initial decay, and indeed practically cannot be detected. A secondary objective of the present work is to understand these puzzling features of the mutual correlation functions in terms of the analytical theory presented below.

As detailed subsequently, the correlation functions analyzed herein are associated with particular orientation mechanisms that do not apply in the case of DNA, so the present results do *not* pertain directly to electric dichroism and birefringence experiments on DNA but do pertain to depolarized dynamic light scattering experiments on DNA. However, we are aware of no depolarized dynamic light scattering data on DNAs with fewer than 250 base pairs, which might qualify as weakly bending rods.

Theory

Basic Formulas for Linear Dichroism and Birefringence and Forward Depolarized Dynamic Light Scattering. The macromolecule is regarded as a linear array of $N + 1$ identical rigid subunits, each of which is connected to its neighbors by identical Hookean twisting and bending springs. These subunits are labeled by the index j ($j = 1, 2, ..., N + 1$). Embedded in each subunit is a body-fixed coordinate frame (x_j, y_j, z_j) chosen such that the z_j-axis lies along the bond vector ($\mathbf{h}_j$) from the jth to ($j + 1$)th subunit. The laboratory frame (x_L, y_L, z_L) is chosen so that in the case of an electric dichroism or birefringence experiment z_L lies along the dc orienting field and in the case of a depolarized dynamic light scattering experiment z_L lies along the direction of polarization of the incident light. Associated with each bond vector is a low-frequency electric polarizability tensor, which is assumed to be axially symmetric about the bond vector with anisotropy, $\Delta\chi = \chi_{\parallel} - \chi_{\perp}$, where $\chi_{\parallel}$ and $\chi_{\perp}$ denote components parallel and perpendicular, respectively, to the bond vector. The local $\Delta\chi_j$ value associated with the bond vector $\mathbf{h}_j$ from the jth to ($j + 1$)th subunit is assumed to be independent of the chain conformation. $\Delta\chi_j$ may represent an azimuthal, or cylindrical, average over the chemical groups constituting the jth subunit. Also associated with each bond vector are a dichroism tensor and an excess optical polarizability tensor, which are likewise assumed to be axially symmetric about the bond vector and independent of chain configuration. The anisotropy of the dichroism tensor is $\Delta a = a_{\parallel} - a_{\perp}$, and that of the excess optical polarizability tensor is $\Delta\alpha = \alpha_{\parallel} - \alpha_{\perp}$, where $a_{\parallel}$ and $a_{\perp}$ denote the molar absorbances, and $\alpha_{\parallel}$ and $\alpha_{\perp}$ the excess optical polarizabilities, for light with polarization parallel or perpendicular, respectively, to the bond vector. For convenience the symbols introduced above, as well as those defined subsequently, are listed in a Symbol Glossary in the Appendix.

The orientation of the macromolecule is assumed to occur via a simple independent induced-dipole mechanism,[2] in which each subunit interacts independently with the external dc electric field, but not with those fields arising from the induced dipoles of the neighboring subunits. Also each subunit is assumed to interact only with the incident light field, but not with the secondary scattered fields arising from other subunits. In addition, the incident light is assumed to exert a completely negligible effect on the orientation of any macromolecule or subunit thereof.

When the external dc electric field is sufficiently weak, the lowest-order contribution to the equilibrium-induced dichroism or birefringence is proportional to E^2, as shown previously.[2] When the system is first equilibrated in a weak external orienting field, and that field is then abruptly turned off, the subsequent relaxation of the dichroism is given by

$$\langle \Delta A(t) \rangle = A_{z_L}(t) - A_{x_L}(t) = cl\langle a_{z_L}(t) - a_{x_L}(t) \rangle \quad (1)$$

where $A_{\mu_L}(t)$ is the absorbance of the sample for light with polarization μ_L (i.e. $\mu_L = z_L$ or x_L) in the laboratory frame, c is the molar concentration of macromolecules, l is the sample path length, and $\langle a_{\mu_L}(t) \rangle$ is the average molar absorbance of a single macromolecule for light with polarization μ_L in the lab frame. The latter can be expressed in terms of the average dichroisms $(a^k_{z_L}(t) - a^k_{x_L}(t))$ of the individual bond vectors (up to order E^2) to yield[2]

$$\langle \Delta A(t) \rangle = cl \sum_{k=1}^{N} \langle a^k_{z_L}(t) - a^k_{x_L}(t) \rangle = cl \frac{\Delta a}{15} \frac{\Delta\chi}{k_B T} E^2 4\pi \sum_{i=1}^{N} \sum_{k=1}^{N} \langle Y_{20}(\Omega_i(0))\, Y_{20}(\Omega_k(t)) \rangle \quad (2)$$

where E is the magnitude of the weak dc orienting field, the $Y_{20}(\Omega)$ denote spherical harmonic functions, and $\Omega_k(t) = (\theta_k(t), \phi_k(t))$ denotes the instantaneous solid angle orientation of the kth bond vector in the laboratory frame. The angular brackets in the first line of eq 2 denote an average over molecules in the nonequilibrium system at time t after the orienting field is turned off, whereas those in the second line denote an average of the indicated correlation function over molecular trajectories of the *equilibrium* system (in the absence of the electric field). In arriving at eq 2, use is made of the relation

$$\langle Y^*_{lm}(\Omega_i(0))\, Y_{LM}(\Omega_k(t)) \rangle = \delta_{l,L}\delta_{m,M} \langle Y_{l0}(\Omega_i(0))\, Y_{l0}(\Omega_k(t)) \rangle \quad (3)$$

which holds for any two bond vectors in the same macromolecule in a fluid with an isotropic equilibrium state.[11]

The corresponding off-field decay of the birefringence after equilibration in the orienting field is given by

$$\langle \Delta n(t) \rangle = \langle n_{z_L}(t) - n_{x_L}(t) \rangle = (2\pi N_A c/(1000 n_0)) \langle \alpha_{z_L}(t) - \alpha_{x_L}(t) \rangle \quad (4)$$

where $n_{\mu_L}(t)$ is the refractive index for light with polarization μ_L in the lab frame, $\langle \alpha_{\mu_L}(t) \rangle$ is the average

excess optical polarizability of a single macromolecule for light with polarization μ_L in the lab frame, N_A is Avogadro's number, and n_0 is the refractive index of the solvent. The quantity $\langle \Delta n(t) \rangle$ is also given by an expression identical to eq 2 except that $a^k_{z_L}(t)$, $a^k_{x_L}(t)$, and Δa are replaced by $\alpha^k_{z_L}(t)$, $\alpha^k_{x_L}(t)$, and $\Delta\alpha$, respectively, and l is replaced by $2\pi N_A/(1000 n_0)$ on the right-hand side.

Clearly, both the dichroism and birefringence probe the same molecular correlation function, which pertains to molecular trajectories *in the absence of any orienting field*. Use of the addition theorem of spherical harmonics and eq 3 allows the correlation function to be written in an alternate form,

$$\sum_{k=1}^{N}\sum_{i=1}^{N} 4\pi \langle Y_{20}(\Omega_k(t))\, Y_{20}(\Omega_i(0)) \rangle = \sum_{k=1}^{N}\sum_{i=1}^{N} \langle P_2(\mathbf{u}_k(t) \cdot \mathbf{u}_i(0)) \rangle \quad (5)$$

where $P_2(x)$ is the Legendre polynomial with rank $l = 2$, and $\mathbf{u}_k(t) = \mathbf{h}_k(t)/|\mathbf{h}_k(t)|$ is the unit vector along the instantaneous bond vector of the kth subunit. The right-hand side of eq 5 can be evaluated directly from the succession of configurations along a Brownian dynamics trajectory,[2-4] as illustrated below.

The simple correlation function in eq 2, and the corresponding expression for the birefringence, applies to the off-field decay after equilibration in a weak electric field by a simple independent induced-dipole orientation mechanism. It does not apply in the case of a permanent dipole orientation mechanism (unpublished results) or a correlated induced dipole mechanism, but does apply to the case of a saturated induced-dipole orientation mechanism.[3] It appears that none of these mechanisms, nor indeed any orientation mechanism that is linear in E^2, is capable of accounting for the observed strong, nearly proportional, dependence of the *relative* amplitude of the fast initial transient on E in the case of DNA. However, Brownian dynamics simulations suggest that, when monopolar forces and molecular translation are included and an orientation mechansim more typical of ion-atmosphere polarization is invoked, DNAs initially perpendicular to the field are induced to form hairpin structures in which the longest "horseshoe" bending mode is enormously enhanced.[12] Although that could potentially account for the strong E dependence of the initial transient, such a topic lies outside the scope of the present work, in part because no succinct theoretical correlation function is available yet to describe the off-field dichroism decay subsequent to such an orientation process. Thus, the present results for off-field decays of the electric dichroism and birefringence are *not* expected to apply to DNA.

A general expression for the autocorrelation function of the depolarized scattered electric field was given previously.[13] In the case of zero-angle depolarized scattering from solutions with an isotropic equilibrium state, this expression reduces to

$$\langle E^{s*}_{x_L}(0)\, E^{s}_{x_L}(t) \rangle = \langle n_V \rangle\, \Delta\alpha (4\pi/15) \sum_{i=1}^{N}\sum_{k=1}^{N} \langle Y_{20}(\Omega_i(0)) Y_{20}(\Omega_k(t)) \rangle \quad (6)$$

where $\langle n_V \rangle$ is the average number of macromolecules in the scattering volume. Equation 6 was also obtained from its precursor by using eq 3. Equation 6 should be applicable to forward depolarized dynamic light scattering from DNA.

Clearly, the off-field decays of the linear electric dichroism and birefringence, subsequent to orientation by an independent induced-dipole mechanism, and the zero-angle depolarized dynamic light scattering all monitor the same molecular mutual-correlation function, more precisely the double sum of subunit correlation functions in eqs 2 and 6.

Basic Theory for the Correlation Functions. The sums of correlation functions in eqs 2 and 6 consist of *self-correlation* functions with $i = k$ and cross-correlation functions with $i \neq k$. Under typical conditions, where at most a single fluorescent photon per macromolecule is detected over a period of many excited state lifetimes of the fluorophore, the fluorescence polarization anisotropy (FPA) probes just the subunit self-correlation functions. In a treatment hereinafter referred to as paper I,[10] it was shown for filaments with mean local cylindrical symmetry that each subunit self-correlation function could be expressed in terms of the mean-squared rotations, $\langle \Delta x_i(t)^2 \rangle$ and $\langle \Delta z_i(t)^2 \rangle$, of that subunit around its body-fixed symmetry (z_i) and transverse (x_i) axes, respectively, in time t.[11] When the transition dipole is rigidly fixed in the ith subunit, one obtains

$$4\pi \langle Y_{20}(\Omega_i(0))\, Y_{20}(\Omega_i(t)) \rangle = \sum_{n=0}^{2} I_n \exp[-(6 - n^2)(\langle \Delta_{xi}(t)^2 \rangle/2) - n^2 (\langle \Delta_{zi}(t)^2 \rangle/2)] \quad (7)$$

wherein $\langle \Delta_{xi}(t)^2 \rangle$ and $\langle \Delta_{zi}(t)^2 \rangle$ pertain to the ith subunit, $I_0 = [(1/2)(3\cos^2\epsilon - 1)]^2$, $I_1 = 3\cos^2\epsilon \sin^2\epsilon$, and $I_2 = (3/4)\sin^4\epsilon$, and ϵ is the polar angle between the transition dipole in the subunit and the local (symmetry) z-axis. When the transition dipole lies along the local symmetry axis, as will be assumed here, one has $\epsilon = 0$ and

$$4\pi \langle Y_{20}(\Omega_i(0)) Y_{20}(\Omega_i(t)) \rangle = \exp[-6\langle \Delta_{xi}(t)^2 \rangle/2] \quad (8)$$

For a filament with mean local cylindrical symmetry, the mean-squared angular displacement of the ith bond vector around the subunit-fixed x_i-axis is independent of the torsional rigidity and therefore identical to that for the same subunit in a corresponding nontwisting filament, since the mean-squared angular displacements around either the x_i- or y_i-axis are identical in any given time interval. Following a previous treatment of weakly bending nontwisting rods,[1] hereinafter referred to as paper II, the displacement of the ith subunit around the x_i-axis in time t is given by $\Delta_{xi}(t) = \theta(t) - \theta(0) + \eta_i(t) - \eta_i(0)$, where $\theta(t) - \theta(0)$ denotes the contribution due to uniform rotation of the end-to-end vector around the rod-fixed x-axis and $\eta_i(t)$ is the angle between the projection of the ith bond vector ($\mathbf{h}_i$) onto the rod-fixed xz-plane and the rod-fixed z-axis, which is taken parallel to the end-to-end vector.

The development in paper I[10] can be generalized to treat subunit cross-correlation functions by focusing not on the rotational motions of individual subunits but instead on the rotational motions of a hypothetical coordinate frame (denoted by superscript H), which is coincident with the frame of the ith subunit at $t = 0$. This hypothetical frame is then imagined to follow a continuous path in both its spatial and angular coordinates as it is very rapidly (practically instantaneously)

translated along the chain from the ith to the kth subunit from time $t = 0$ to t', being successively coincident with the coordinate frame of each intermediate subunit as it passes by. The rotational dynamics of such hypothetical coordinate frames, as they translate rapidly along the effectively stationary but instantaneously deformed filaments, is a Gaussian random process that is statistically equivalent to any normal Brownian motion, although it takes place in an arbitrarily small time t'. Upon arrival at and coincidence with the frame of the kth subunit, the hypothetical frame simply follows the subsequent natural Brownian trajectory of that kth subunit from time t' to t. The total angular displacement of this hypothetical frame around its body-fixed x-axis in time $t > t'$ is given by

$$\begin{aligned}\Delta^{H}_{x,ik}(t) &= \Delta_{xk}(t') - \Delta_{xi}(0) + \Delta_{xk}(t) - \Delta_{xk}(t') \\ &= \Delta_{xk}(t) - \Delta_{xi}(0)\end{aligned} \tag{9}$$

wherein the time t' for translation of the hypothetical frame from the ith to the kth subunit is understood to be so small that $\Delta_{xk}(t') = \Delta_{xk}(0)$. The quantity $\Delta^{H}_{x,ik}(t)$ has several essential properties that are formally identical to that, $\Delta_{xi}(t)$, of a single subunit, namely (1) it is a continuous single-valued function of the time, (2) its mean value over any interval δt in the interval 0 to t vanishes, (3) it is uncorrelated with the concurrent rotations, $\Delta^{H}_{y,ik}(t)$ and $\Delta^{H}_{z,ik}(t)$, of that same hypothetical frame around its other body-fixed axes over any interval δt in the interval 0 to t, and its variance $\langle\Delta^{H}_{x,ik}(t)^2\rangle$ is a continuous monotonically increasing function of the time. As in the previous development,[10] these properties suffice to derive the conditional probability per unit Euler angle ($G(\Phi^{H}_{ik}(t)\ t|\Phi^{H}_{ik}(0)\ 0)$) that such a hypothetical frame with initial laboratory Euler orientation $\Phi^{H}_{ik}(0)$, which is coincident with the frame of the ith subunit at $t = 0$, has evolved in time t to the laboratory Euler orientation $\Phi^{H}_{ik}(t)$, which is coincident with the frame of the kth subunit at time t. For a system with an isotropic equilibrium state, the result is

$$\begin{aligned}&G(\Phi^{H}_{ik}(t)\ t|\Phi^{H}_{ik}(0)\ 0) = \\ &\sum_{l}\sum_{m}\sum_{n}[(2l+1)/8\pi^2]\exp[-(l(l+1) - m^2)\langle\Delta^{H}_{x,ik}(t)^2\rangle/2] \times \\ &\qquad \exp[-m^2\langle\Delta^{H}_{z,ik}(t)^2\rangle/2]D^{l*}_{m\,n}(\Phi^{H}_{ik}(0))\,D^{l}_{mn}(\Phi^{H}_{ik}(t))\end{aligned} \tag{10}$$

In eq 10, the rotation functions, $D^{l}_{mn}(\Phi) = D^{l}_{mn}(\alpha\beta\gamma) = \exp[in\alpha]\ d^{l}_{mn}(\beta)\ \exp[im\gamma]$, are taken in the convention of Wigner[14] and Edmonds.[15] By using the averaging protocols employed previously,[10,11] we obtain

$$\begin{aligned}\langle D^{L}_{MN}(\Phi^{H}_{ik}(0))\,D^{l*}_{m\,n}(\Phi^{H}_{ik}(t))\rangle &= \delta_{lL}\delta_{mM}\delta_{nN}(2l+1)^{-1} \times \\ &\exp[-(l(l+1) - m^2)\langle\Delta^{H}_{x,ik}(t)^2\rangle/2] \times \\ &\exp[-m^2\langle\Delta^{H}_{z,ik}(t)^2\rangle/2]\end{aligned} \tag{11}$$

Let $\omega_R = (\epsilon, 0)$ denote the orientation of a vector fixed in the hypothetical frame and $\omega_L = (\xi(t), \sigma(t))$ its instantaneous orientation in the lab frame. Then,

$$Y_{lm}(\omega_L(t)) = \sum_{n=-l}^{l} D^{l}_{nm}(\Phi^{H}_{ki}(t))\,Y_{ln}(\omega_R) \tag{12}$$

Upon making use of eq 11, one obtains

$$\begin{aligned}&4\pi\langle Y_{2m}(\omega_L(0))\,Y^{*}_{2m}(\omega_L(t))\rangle = \\ &\sum_{n=0}^{2} I_n \exp[-(6 - n^2)\langle\Delta^{H}_{x,ik}(t)^2\rangle/2]\exp[-n^2\langle\Delta^{H}_{z,ik}(t)^2\rangle/2]\end{aligned} \tag{13}$$

where the I_n are given after eq 7. We now take the vector under consideration to be the z-axis of the hypothetical frame, in which case its lab orientation at $t = 0$ is $\omega_L(0) = \Omega_i(0)$ and its lab orientation at time $t > t'$ is $\omega_L(t) = \Omega_k(t)$. In addition, $\epsilon = 0$, so $I_0 = 1.0$, and $I_1 = 0 = I_2$. Now the desired cross-correlation function becomes

$$4\pi\langle Y_{20}(\Omega_i(0))\,Y_{20}(\Omega_k(t))\rangle = \exp[-6\langle\Delta^{H}_{x,ik}(t)^2\rangle/2] \tag{14}$$

Thus, the pertinent correlation function is now expressed in terms of the mean-squared angular displacement of the hypothetical frame around its body-fixed x-axis. The limit $t' \to 0$ is assumed to apply in eq 14, so the hypothetical frame is coincident with that of the kth subunit for all $t > 0$.

The evaluation of $\langle\Delta^{H}_{x,ik}(t)^2\rangle$ is performed using the normal mode theory for a weakly bending nontwisting rod that was presented in paper II.[1] As remarked earlier, for a filament with mean local cylindrical symmetry, the mean-squared angular displacements of the subunits i and k around their body-fixed x_i- and x_k-axes, respectively, are identical to those for the corresponding subunits in a filament that undergoes no twisting whatsoever. Hence, the net angular displacement of the hypothetical frame around its body-fixed x-axis is given by

$$\Delta^{H}_{x,ik}(t) = \theta(t) - \theta(0) + \eta_k(t) - \eta_i(0) \tag{15}$$

where $\theta(t) - \theta(0)$ is the contribution due to uniform rotation of the end-to-end vector around the rod-fixed x-axis, and $\eta_k(t)$ is the angle between the projection of the kth bond vector ($\mathbf{h}_k$) onto the rod-fixed xz-plane and the rod-fixed z-axis, which is taken parallel to the end-to-end vector. Making use of eqs 3 and 25 of paper II to express $\eta_k(t)$ and $\eta_i(0)$ in terms of the amplitudes ($\varrho(t)$) of the normal modes (right eigenvectors) of the dynamical operator, one obtains

$$\begin{aligned}\Delta^{H}_{x,ik}(t) = \theta(t) - \theta(0) + \frac{1}{h}\sum_{l=3}^{N}[&(Q_{k+1,l} - Q_{kl})\varrho_l(t) - \\ &(Q_{i+1,l} - Q_{il})\varrho_l(0)]\end{aligned} \tag{16}$$

wherein the Q_{kl} are elements of the normal coordinate transformation matrix that diagonalizes the dynamical operator, and can be determined according to eq 79 of paper II, and h is the constant bond length. Making further use of eqs 59 and 85 from paper II and the statistical independence of the normal modes yields, finally

$$\begin{aligned}\langle(\Delta^{H}_{x,ik}(t))^2\rangle = 2D_R t + (h/P)\sum_{l=3}^{N}[&(Q_{k+1,l} - Q_{kl})^2 + \\ &(Q_{i+1,l} - Q_{il})^2 - 2(Q_{k+1,l} - Q_{kl})(Q_{i+1,l} - Q_{il})e^{-t/\tau_l}]\end{aligned} \tag{17}$$

wherein $P = \kappa_h h/k_B T$ is the dynamic persistence length, $k_B T$ is thermal energy, κ_h is the dynamic bending constant, $\tau_l = fh^3/(k_B T P \Lambda_l)$ is the relaxation time of the lth bending normal mode, $f = 6\pi\eta h/2$ is the subunit

friction factor, and Λ_l is the particular eigenvalue of the dynamical matrix.

The normalized dichroism decay, $\langle \Delta A(t) \rangle / \langle \Delta A(0) \rangle$, is computed by inserting eq 17 into eq 14, which is in turn substituted in eq 2, and then dividing by $\langle \Delta A(0) \rangle$. The birefringence decay and field autocorrelation function of the forward depolarized dynamic light scattering are similarly computed using, respectively, the birefringence analogue of eq 2 or 6.

Brownian Dynamics Simulations. Brownian dynamics simulations of discrete wormlike chains with preaveraged hydrodynamic interactions are carried out using the model potential and procedures described previously.[1-4,7-9] Self-correlation functions from such simulations were previously compared to those derived from the normal mode theory in paper II,[1] and excellent agreement was obtained within the domain of validity of the normal mode theory, namely $L \lesssim (0.6)P$, where L is the contour length and P the dynamic persistence length. The normalized dichroism decay, $\langle \Delta A(t) \rangle / \langle \Delta A(0) \rangle$, is calculated via eqs 5 and 2 directly from the simulated trajectories under the assumption that the time series is stationary, in which case the ensemble average can be replaced by an average over initial times with the same time delay (t) between $\mathbf{u}_i(\tau)$ and $\mathbf{u}_k(\tau + t)$. A more detailed description of the protocol is provided elsewhere.[3]

Model Parameters. Essential parameters in the model are the bead diameter $h = 31.8$ Å, dynamic persistence length $P = 2000$ Å, temperature $T = 293$ K, solvent viscosity $\eta = 0.01$ P, and translational friction factor per subunit $f = 6\pi\eta h/2 = 3.00 \times 10^{-8}$ erg s. The normalized dichroism decay is both calculated and simulated for two different chains consisting of 27 subunits ($L = 859$ Å) and 39 subunits ($L = 1240$ Å). Each of these falls within the domain of validity of the normal mode theory ($L \leq (0.6)P$). The model used in the Brownian dynamics simulation also experiences a Hookean bond-stretching potential with a fairly stiff force constant, $g = 40$ dyne cm^{-1}. The uniform rotational diffusion coefficient (D_R) used in the normal mode theory is calculated from the average best-fit longest relaxation time (τ_R) in the Brownian dynamics simulations according to $D_R = 1/(6\tau_R)$. This value differs slightly from the D_R calculated according to the normal mode theory. The difference presumably arises from the slightly different end-to-end lengths of the rods in the Brownian dynamics simulations, which exhibit variously bent and slightly stretched or compressed configurations.

Results and Discussion

The calculated and simulated normalized dichroism decays, $\langle \Delta A(t) \rangle / \langle \Delta A(0) \rangle$, are compared for the 27 and 39 subunit chains in Figures 1 and 2, respectively. In each case, the calculated curves agree with the simulated data within the statistical errors in the latter. Double exponential expressions of the form,

$$\langle \Delta A(t) \rangle / \langle \Delta A(0) \rangle = a_f \exp[-t/\tau_f] + a_R \exp[-t/\tau_R] \quad (18)$$

were fitted to both the calculated and simulated curves subject to the constraint, $a_f + a_R = 1.0$. The best-fit relaxation times and amplitudes are indicated in Table 1. The agreement between the simulated and calculated curves in regard to the amplitude, a_R, and relaxation time, τ_R, of the main relaxation is excellent, as expected. Agreement with respect to the amplitude, a_f, and

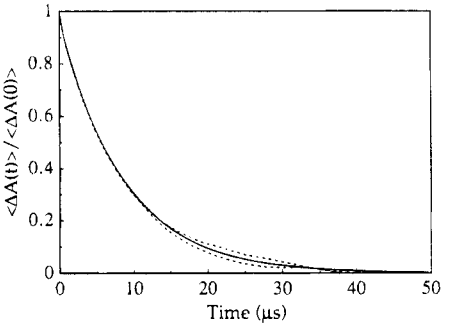

Figure 1. Normalized off-field dichroism decays, $\langle \Delta A(t) \rangle / \langle \Delta A(0) \rangle$, versus time for the 27 subunit chains. The dashed curves represent the simulated data, and the solid curve represents the analytical theory. Essential parameters are $h = 31.8$ Å, $P = 2000$ Å, $T = 293$ K, and $\eta = 0.01$ P.

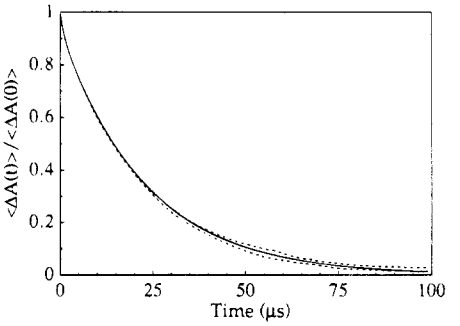

Figure 2. Normalized off-field dichroism decays, $\langle \Delta A(t) \rangle / \langle \Delta A(0) \rangle$, versus time for the 39 subunit chains. The dashed curves represent the simulated data, and the solid curve represents the analytical theory. Essential parameters are $h = 31.8$ Å, $P = 2000$ Å, $T = 293$ K, and $\eta = 0.01$ P.

Table 1. Best-Fit Amplitudes and Relaxation Times Obtained by Fitting Eq 18 to Either Normal Mode Theory (NMT) or Brownian Dynamics Simulations (BDS)

data	N (subunits)	P (Å)	a_f	τ_f (ns)	a_R	τ_R (ns)
NMT	27	2000	0.0346	267	0.965	8600
NMT	39	2000	0.0641	1004	0.936	22900
BDS	27	2000	0.03 (0.01)	210 (50)	0.97 (0.01)	8600 (200)
BDS	39	2000	0.06 (0.01)	1100 (100)	0.94 (0.01)	22900 (700)

relaxation time, τ_f, of the fast initial transient is satisfactorily within, or nearly within, the statistical errors of the simulations. At this double-exponential level of resolution, the analytical theory embodied in eqs 14 and 17 evidently gives a satisfactory account of the correlation functions manifested in the zero-angle depolarized dynamic light scattering and in the off-field decays of the dichroism or birefringence subsequent to equilibrium orientation in a weak electric field by a simple, independent, induced dipole mechanism. This conclusion achieves a primary objective of the present work.

An advantage of the analytical formulation is that it allows in some cases a further dissection of the problem and additional insights into the origins of the fitted parameters. In this regard, it is pertinent to inquire how the *best-fit* amplitude, a_f, of the fast initial transient compares with the *theoretical* fraction of the amplitude that is relaxed by the bending normal modes, which is given by

$$a_b = 1 - \lim_{t \to \infty} (e^{6D_R t} \langle \Delta A(t) \rangle / \langle \Delta A(0) \rangle) \quad (19)$$

For the chain with $N + 1 = 27$ subunits, one has $a_f =$

Table 2. Comparison of Best-Fit τ_f with Relevant Relaxation Times in the Theory

N	τ_f (ns)	τ_R (ns)	τ_3 (ns)	τ_4 (ns)	τ_5 (ns)
27	267	8600	664	96	28
39	1004	22900	2543	363	103

0.0346 from the fit in Table 1, while the exact value, $a_b = 0.0339$, is calculated from eq 19. These amplitudes are nearly identical, as expected. For $N + 1 = 39$ subunits one has $a_f = 0.0641$ and $a_b = 0.0659$, which are also virtually identical. The fast component in the double-exponential fitting program is evidently reporting quite accurately the total amplitude of relaxation due to the bending normal modes.

It is also relevant to compare the theoretical fractional amplitude, a_b, of the rapid initial transient in the mutual-coorelation function with that in the corresponding self-coorelation function (averaged over all subunits), which is given by[18]

$$b_b = 1 - (Z_0)^{1/2} \exp[-Z_0/3](\pi^{1/2}/2)\,\mathrm{erf}(Z_0^{1/2}) \quad (20)$$

where $Z_0 = 6L/4P$, and $L = (N + 1)(31.8 \times 10^{-8}$ cm) is the contour length. One obtains $b_b = 0.338$ for $N + 1 = 27$ subunits and $b_b = 0.437$ for 39 subunits. In either case, b_b exceeds a_b by about 7-fold or more. Hence, a great deal of cancelation must occur in the double sums of the cross-correlation functions.

The connection between the best-fit relaxation time of the fast initial transient and the various bending normal mode relaxation times is also a matter of considerable interest. The relevant data are compared in Table 2. For both rods, τ_f lies between the relaxation times of the longest and second longest bending normal modes, τ_3 and τ_4, respectively. Interestingly, τ_f is very nearly the geometric mean of τ_3 and τ_4. It is somewhat surprising that τ_f is so much smaller than τ_3, because the $l = 3$ normal mode accounts for more than half of the total mean-squared angular displacement of those subunits near the chain ends, where the amplitude of motion is greatest.

Both the small fractional amplitude of the initial transient in the mutual correlation function and the apparent loss of amplitude of the term with $1/\tau_3$ relaxation rate relative to other terms with $1/\tau_4$ and/or $2/\tau_3$ relaxation rates can be understood in the following way. That part of $\exp[-6\langle\Delta^H_{x,ik}(t)^2\rangle/2]$ due to bending of the filament (i.e. originating from the second term in eq 17) is expanded to first order in the ratio of the bond length to the persistence length, h/P. This expansion is performed for both $\langle\Delta A(t)\rangle$ and $\langle\Delta A(0)\rangle$. After some rearrangement one obtains

$$e^{6D_R t}\langle\Delta A(t)\rangle/\langle\Delta A(0)\rangle \cong 1 - (6h/P)\sum_{l=3}^{N} B_l\,(1 - e^{-t/\tau_l}) + \mathcal{O}((h/P)^2) \quad (21)$$

where

$$B_l = \frac{\sum_{i=1}^{N}\sum_{j=1}^{N}(Q_{i+1,l} - Q_{il})(Q_{j+1,l} - Q_{jl})}{\sum_{p=1}^{N}\sum_{q=1}^{N}\{1 - (6h/P)\sum_{m=3}^{N}[(Q_{p+1,m} - Q_{pm})(Q_{q+1,m} - Q_{qm})]^2\}} \quad (22)$$

When the coefficients B_l in eq 21 are evaluated numerically, those for the odd-l normal modes, including $l = 3$, are found to vanish within the limits of computer truncation errors. In fact, $\sum_{i=1}^{N}(Q_{i+1,l} - Q_{il})$ rigorously vanishes for any odd-l mode by symmetry for the following reason. The elements Q_{il} denote the relative displacements of the subunits i in the y-direction (perpendicular to the end-to-end vector $\hat{\mathbf{z}}$) for the lth normal mode. For the odd-l modes, the Q_{il} are symmetric about the center of the filament, so $Q_{il} = Q_{N+1-(i-1),l} = Q_{N-i+2,l}$. The difference, $Q_{i+1,l} - Q_{il}$, which is proportional to the angle between the bond vector from the ith to the $(i + 1)$th subunit projected onto the yz-plane and the end-to-end vector $\hat{\mathbf{z}}$, is then antisymmetric about the center of the filament. That is, $Q_{i+1,l} - Q_{il} = Q_{N-(i+1)+2,l} - Q_{N-i+2,l} = -(Q_{N-i+2,l} - Q_{N-i+1,l})$. Consequently, the sum over such angular displacements rigorously vanishes for all odd-l modes. Thus, to lowest order in h/P, the relaxation rate $1/\tau_3$ does not appear at all. Although not eliminated rigorously by symmetry, the sums $\sum_{i=1}^{N}(Q_{i+1,l} - Q_{il})$ for even-l modes are rather small, due to near cancelation of the terms in each half-filament. Indeed, in the absence of hydrodynamic interactions the even-l sums would also vanish. The main contributions of bending modes to the relaxing amplitude come then from the small first-order (proportional to h/P) contribution of the $l = 4$ mode and from the second-order (proportional to $(h/P)^2$) contributions of the $l = 3$ mode. Although both $1/\tau_3$ and $2/\tau_3$ relaxation rates appear among the second-order terms, the amplitude of the latter dominates that of the former. The main conclusion of this analysis is that the summation over i, k in the relevant mutual correlation functions in eqs 2 and 6 yields a great deal of cancelation. Consequently, the fraction of the total amplitude relaxed by all bending motions is much smaller than in the case of the self-correlation functions. Moreover the amplitude of the term relaxing with rate $1/\tau_3$ is greatly reduced compared to that of the $1/\tau_4$ and $2/\tau_3$ terms. Under these conditions, the best-fit relaxation time for the initial transient is not simply related to either τ_3 to τ_4, but lies between those. This explanation was tested quantitatively in the following way. First, the expanded (up to h/P) dichroism ratio in eq 21 was fitted by eq 18. The slow component exhibits $\tau_R = 8600$ ns, as expected, but the amplitude and relaxation time of the fast component are $a_f = 0.015$ and $\tau_f = 90$ ns, which is close to $\tau_4 = 96$ ns. This indicates that the τ_4 term dominates the first-order h/P contribution and amounts to 1.5% of the total amplitude. We now assume that the $2/\tau_3$ term dominates the second- and higher-order contributions and comprises the remaining 2.0% of the total relaxing amplitude ($a_f = 0.035$). The implied dichroism ratio would then be

$$\langle\Delta A(t)\rangle/\langle\Delta A(0)\rangle = 0.965\exp[-t/\tau_R] + 0.015\exp[-t/\tau_4] + 0.020\exp[-2t/\tau_3] \quad (23)$$

When eq 23 is fitted by a double exponential, the amplitude and relaxation time of the fast component are now $a_f = 0.037$ and $\tau_f = 221$ ns, which correspond fairly closely to the results in the first line of Table 1. This demonstrates that the fast decay arises primarily from the first-order (in h/P) term with relaxation time τ_4 and a term of comparable amplitude with relaxation time $\tau_3/2$ that arises from second- and higher-order (in h/P) contributions. A similar conclusion applies also for the longer chain (data not shown).

In order to obtain $\tau_f \approx \tau_3$, it is necessary for the orienting electric field to induce preferentially a very much larger amplitude of the $l = 3$ "horseshoe" mode, as occurs in the orientation mechanism(s) proposed by Elvingson for DNA molecules.[12] A previous analysis[6] of rapid initial transients in the off-field dichroism decays[16,17] for DNAs containing 100−250 bp is predicated on the assumption that $\tau_f = \tau_3$ and is valid *only* in the event that the relative amplitude of the longest bending mode is greatly enhanced by the prevailing orientation mechanism.

It is also of interest to compare the *theoretical* initial slope of the normalized dichroism decay, or zero-angle depolarized light scattering correlation function, which is computed from the time derivative of eq 17, with that computed from the parameters of the best double-exponential fit in Table 1. The former protocol gives $[\partial(\Delta A(t)/\Delta A(0))/\partial t]_{t=0} = 1.27 \times 10^6\ s^{-1}$, while the latter gives $2.72 \times 10^5\ s^{-1}$. Evidently, the theoretical initial slope consists of components much faster than are manifested in the double-exponential fit, as expected from the fact that $\tau_l \leq \tau_f$ for all $l \geq 4$, and the fact that higher order terms (in h/P) contribute significantly to the initial slope despite their small contribution to the amplitude of the rapid initial transient.

Within its domain of validity, the analytical theory is much better suited to fitting experimental data than are Brownian dynamics simulations. The latter are so expensive in terms of cpu time that their use for iterative data fitting in some cases may be impractical. Also, due to their finite statistical errors, "convergence" of the adjustable parameters to precise values is neither smooth nor unique. In using the analytical theory, the computationally expensive step is the diagonalization of the dynamical matrix and the determination of the transformation matrix elements Q_{il}. Since the dynamical matrix contains none of the model parameters, and its dimensionality is the number of subunits $N + 1$, which remains constant for filaments of fixed length, its eigenvalues and transformation vectors need to be determined only once for a given filament, and simply used in each iteration of the data fitting.[1] Thus, data analysis using the analytical theory proceeds quite rapidly, despite its apparent complexity. The importance of testing the analytical theory in the data analysis code by means of Brownian dynamics simulations can hardly be overestimated.

As demonstrated above, the analytical theory admits a dissection of the results and depth of analysis that is a useful adjunct to Brownian dynamics simulations.

Finally, the extensive cancelation of terms in the mutual correlation functions severely reduces the relative contribution of the bending modes to the relaxation, and somewhat complicates the interpretation of the data. Except in those cases where the amplitude of the longest bending mode is preferentially driven or enhanced by the orienting field, it appears that experimental techniques that probe self- rather than mutual-rotational correlation functions may provide superior experimental access to the bending dynamics of weakly bending filaments.

Acknowledgment. This work was supported in part by a grant, MCB-9317042 from the National Science Foundation.

Appendix. Symbol Glossary

$\Delta a = a_{\parallel} - a_{\perp}$	anisotropy of the dichroism tensor associated with each bond vector
$a_{z_L}(t) - a_{x_L}(t)$	instantaneous dichroism of a single macromolecule in the laboratory frame
$a^k_{z_L}(t) - a^k_{x_L}(t)$	instantaneous dichroism of the kth bond vector in the laboratory frame
$\Delta A(t) = A_{z_L}(t) - A_{x_L}(t)$	instantaneous dichroism of the solution in the laboratory frame
$\Delta\alpha = \alpha_{\parallel} - \alpha_{\perp}$	anisotropy of the excess optical polarizability associated with each bond vector
$\alpha_{z_L}(t) - \alpha_{x_L}(t)$	instantaneous excess optical polarizability of a single macromolecule in the laboratory frame
$\alpha^k_{z_L}(t) - \alpha^k_{x_L}(t)$	instantaneous excess optical polarizability of the kth bond vector in the laboratory frame
a_f, a_R	best-fit amplitudes of fast and slow components, respectively, in a double-exponential fit to the correlation function
a_b	theoretical fraction of the mutual correlation function amplitude that is relaxed by bending modes
$\alpha\beta\gamma$	component rotations of a Euler rotation $\Phi = (\alpha\beta\gamma)$
b_b	theoretical fraction of the self-correlation function amplitude that is relaxed by bending modes
B_l	coefficients of $(1 - \exp[-t/\tau_l])$ terms in the first-order expansion of the bending contribution to the dichroism
c	molar concentration of macromolecules
$D^l_{mn}(\Phi)$	Wigner rotation function of the Euler angle $\Phi = (\alpha\beta\gamma)$
D_R	rotational diffusion coefficient for end-over-end tumbling
δ_{lm}	Kronecker delta
E	amplitude of orienting electric field
$E^s_{x_L}(t)$	electric field of forward depolarized scattered light
f	friction factor of subunit
$(G(\Phi^H_{ik}(t)\ t\|\Phi^H_{ik}(0)\ 0))$	probability per unit Euler angle that the hypothetical frame with laboratory orientation $\Phi(0)$ at time 0 has laboratory orientation $\Phi(t)$ at time t
$\mathbf{h}_j$	bond vector of jth subunit
h	bond vector length
I_0, I_1, I_2	trigonometric weighting factors given after eq 5
κ_h	dynamic bending constant
k_B	Boltzmann constant
l	optical path length of the sample
L	contour length of the weakly bending rod
Λ_l	eigenvalue of the lth bending normal mode of the dynamical matrix
n_0	refractive index of the solvent
$\Delta n(t) = n_{z_L}(t) - n_{x_L}(t)$	instantaneous birefringence of the sample
N_A	Avogadro's number

$n_v = cV$	average number of macromolecules in scattering volume V
$\eta_j(t)$	instantaneous angle between the projection of $\mathbf{h}_j$ onto the rod-fixed xz plane and the rod-fixed z-axis
η	solvent viscosity
$\theta(t) - \theta(0)$	contribution of uniform end-over-end tumbling to $\Delta_{xi}(t)$
P	persistence length
$P_2(x)$	Legendre polynomial with rank $l = 2$
Q_{kl}	element of the matrix that diagonalizes the dynamical matrix operator by similarity transformation
t	time
T	absolute temperature
τ_l	relaxation time of the lth bending mode
τ_f, τ_R	best-fit relaxation times of fast and slow components, respectively, in a double-exponential fit to the correlation function
$\mathbf{u}_j(t) = \mathbf{h}_j/h$	unit vector along the jth bond vector
$\omega_R = (\epsilon, 0)$	solid angle orientation of a vector fixed in the hypothetical frame
$\omega_L = (\xi(t), \zeta(t))$	solid angle orientation of the same (above) vector in the laboratory frame
x_j, y_j, z_j	coordinate frame of the jth subunit
x_L, y_L, z_L	coordinate frame of the laboratory
$\langle \Delta x_j(t)^2 \rangle$ and $\langle \Delta z_j(t)^2 \rangle$	mean-squared angular displacement of the jth subunit around its body-fixed x_j- and z_j-axes, respectively, in time t
$\langle (\Delta^H_{x,ik}(t))^2 \rangle$, $\langle (\Delta^H_{z,ik}(t))^2 \rangle$	mean-squared angular displacements of the hypothetical frame around its body-fixed x- and z-axes, respectively, in time t
$\Delta\chi = \chi_{\parallel} - \chi_{\perp}$	anisotropy of the low-frequency electric polarizability tensor associated with each bond vector
$Y_{l0}(\Omega_k(t))$	spherical harmonic function of the solid angle $\Omega(t) = (\theta(t), \phi(t))$
Z_0	parameter in eq 20 ($Z_0 = 6L/4P$)

References and Notes

(1) Song, L.; Allison, S. A.; Schurr, J. M. *Biopolymers* **1990**, *29*, 1773.
(2) Lewis, R. J.; Allison, S. A.; Eden, D.; Pecora, R. *J. Chem. Phys.* **1988**, *89*, 2490.
(3) Allison, S. A.; Nambi, P. *Macromolecules* **1992**, *25*, 759.
(4) Allison, S. A.; Austin, R. H.; Hogan, M. E. *J. Chem. Phys.* **1989**, *90*, 3843.
(5) Song, L.; Schurr, J. M. *Biopolymers* **1990**, *30*, 229.
(6) Hustedt, E. J.; Spaltenstein, A.; Kirchner, J. J.; Hopkins, P. B.; Robinson, B. H. *Biochemistry* **1992**, *32*, 1774.
(7) Allison, S. A.; McCammon, J. A. *Biopolymers* **1984**, *23*, 363.
(8) Allison, S. A. *Macromolecules* **1986**, *19*, 118.
(9) Allison, S. A.; Sorlie, S. S.; Pecora, R. *Macromolecules* **1990**, *23*, 1110.
(10) Schurr, J. M. *Chem. Phys.* **1984**, *84*, 71.
(11) Schurr, J. M.; Fujimoto, B. S.; Wu, P.; Song, L. In *Topics in Fluorescence Spectroscopy, Volume 3: Biochemical Applications*; Lakowicz, J. R., Ed.; Plenum Press: New York, 1992.
(12) Elvingson, C. *Biophys. Chem.* **1992**, *43*, 9.
(13) Schurr, J. M. *CRC Crit. Rev. Biochem.* **1977**, *4*, 371.
(14) Wigner, E. P. *Group Theory*; Academic Press: New York, 1959.
(15) Edmonds, A. R. *Angular Momentum in Quantum Mechanics*; Princeton University Press: Princeton, NJ, 1974.
(16) Diekmann, S.; Hillen, W.; Morgenmeyer, B.; Wells, R. D.; Pörschke, D. *Biophys. Chem.* **1982**, *15*, 263.
(17) Pörschke, D.; Zacharias, W.; Wells, R. D. *Biopolymers* **1987**, *26*, 271.
(18) Wu, P.; Fujimoto, B. S.; Schurr, J. M. *Biopolymers* **1988**, *26*, 1463.
(19) Aragón, S.; Pecora, R. *Macromolecules* **1985**, *18*, 1868.
(20) Aragón, S. *Macromolecules* **1987**, *20*, 370.
(21) Aragón, S.; Luo, R. *Proc. SPIE—Int. Soc. Opt. Eng.* **1991**, *1430*, 65.
(22) Aragón, S. *Proc. SPIE—Int. Soc. Opt. Eng.* **1993**, *1884*, 33.

MA946375K